Influence of Angle of Attack on the Aerodynamic Efficiency and Stall Characteristics of a 3D-Printed Flat-Plate Glider at a Freestream Velocity of 8 m/s: A Computational Fluid Dynamics Study

Ayaan Kaushal

Abstract: ***This study investigates the influence of angle of attack on the aerodynamic performance and stall characteristics of a 3D-printed flat-plate glider using Computational Fluid Dynamics (CFD). Steady-state simulations were conducted over an angle-of-attack range of 0° to 30° in 2° increments at a constant freestream velocity of 8 m/s. Lift coefficient (CL), drag coefficient (CD), and aerodynamic efficiency (CL/CD) were evaluated for each simulation. Lift increased approximately linearly within the pre-stall region before reaching a maximum near 24° to 26°, after which flow separation reduced lift while drag continued to increase. Maximum aerodynamic efficiency occurred at approximately 6°, indicating that optimum glide performance occurs well before stall. The findings improve understanding of low-Reynolds-number flat-plate aerodynamics and demonstrate the usefulness of CFD as a cost-effective tool for preliminary aircraft design and aerodynamic performance evaluation.***

Keywords: Computational Fluid Dynamics; Angle of Attack; Aerodynamic Efficiency; Stall; Flat-Plate Glider; Lift Coefficient; Drag Coefficient; Low-Reynolds-Number Aerodynamics

1. Introduction

1.1 Background

Gliders are aircraft that rely solely on aerodynamic forces to remain airborne without continuous propulsion. [3,4] Unlike powered aircraft, gliders must maximize aerodynamic efficiency to convert altitude into horizontal distance travelled. Consequently, understanding the relationship between lift, drag, and angle of attack is fundamental to improving glider performance. Modern Computational Fluid Dynamics (CFD) enables engineers to analyse airflow around aircraft without expensive wind tunnel testing, making it a valuable tool in preliminary aerodynamic design. [3,5]

Although CFD has been widely used to investigate the aerodynamic performance of conventional airfoils, comparatively few studies examine the aerodynamic behaviour of simple flat-plate gliders manufactured using consumer-grade 3D printing. [1, 2, 6, 7, 8] These lightweight gliders are commonly used in educational projects, rapid prototyping, and preliminary aircraft design yet their aerodynamic characteristics remain less well documented than those of traditional cambered airfoil-based wings. In particular, the relationship between angle of attack, aerodynamic efficiency and stall behaviour for a flat-plate glider requires further investigation. A better understanding of these relationships can assist in identifying operating conditions that maximize glide performance while avoiding aerodynamic stall.

1.2 Scope

This investigation evaluates the influence of angle of attack on the aerodynamic performance of a single 3D-printed flat-plate glider using steady state CFD simulations. The study considers angles of attack between 0° and 30° at a constant freestream velocity of 8 m/s while maintaining the same glider geometry, material properties, and atmospheric conditions throughout all simulations.

The investigation focuses on three aerodynamic performance metrics:

- Lift coefficient (CL)
- Drag coefficient (CD)
- Aerodynamic efficiency (CL/CD)

The stall angle is identified by examining changes in the lift coefficient together with pressure contours, velocity contours, and streamline visualizations.

The study does not investigate the effects of changing Reynolds number, airspeed, wing geometry, material properties, structural deformation, control surfaces, wind gusts, or transient flight conditions. Experimental validation through wind-tunnel or flight testing is also beyond the scope of this investigation.

Lift
Lift is the aerodynamic force perpendicular to airflow. [3,4,15,19] The lift coefficient (CL) is a unitless number that measures how well an object, like an airplane wing, turns moving air or fluid into an upward lifting force.[3] Lift is affected by AoA as increasing it changes the pressure distribution.

$$Coefficient\ of\ Lift\ (CL) = \frac{L}{\frac{1}{2}\rho V^2 A}$$

L is lift, ρ is fluid density, V is velocity, and A is surface area. [3,15]

Drag
Drag is a mechanical force that opposes motion. [3, 4, 15, 19] The drag coefficient is a number that shows how much an object resists moving through a fluid like air or water. It

depends on the shape of the object, its tilt, and how the fluid flows around it.

$$Coefficient\ of\ Drag\ (CD) = \frac{D}{\frac{1}{2}\rho\, V^2 S}$$

D is drag force, ρ is fluid density, V is velocity, and S is reference area. [3,15]

Aerodynamic Efficiency

Aerodynamic efficiency is the ratio of Lift to Drag.[3] From it, the efficiency of a glider can be judged.

$$Aerodynamic\ Efficiency\ (L/D) = \frac{Coefficient\ of\ Lift\ (CL)}{Coefficient\ of\ Drag\ (CD)}$$

Stall

Increasing the AoA initially increases lift but beyond critical AoA, flow separation occurs where lift decreases and drag increases. [3, 9, 14] This point is called the stall angle.

Table 1: Glider Design and Geometry

Parameter	Value
Wingspan	130.000 mm
Chord Length	31.000 mm
Wing Area	3986.000 mm²
Thickness	0.300 mm
Material	Polylactic Acid
Mass	3.565 g
Aspect Ratio	4.24

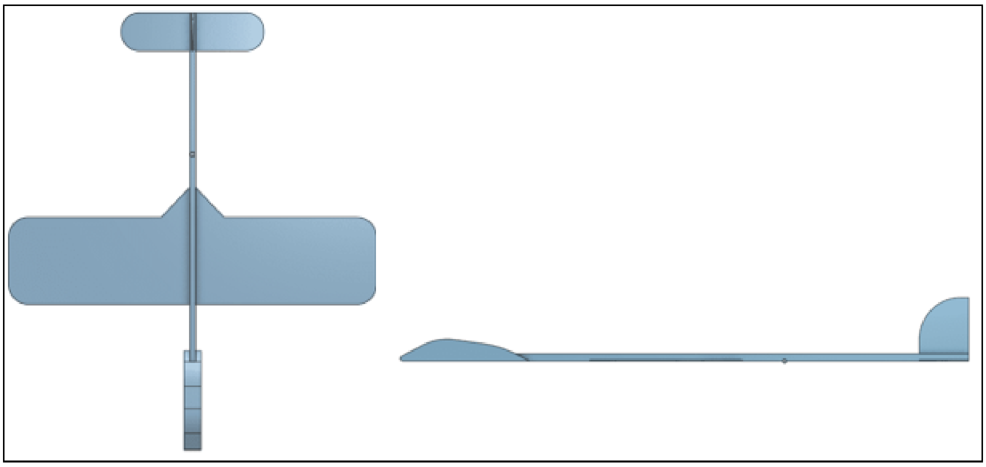

Figure 1: CAD View of Glider (Side and Top- Down View).

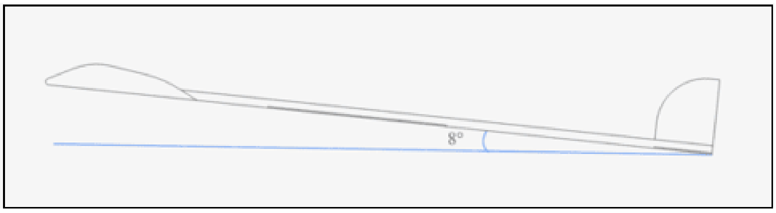

Figure 2: Angle of attack example of the glider (blue lines for reference showing the AoA to be 8°).

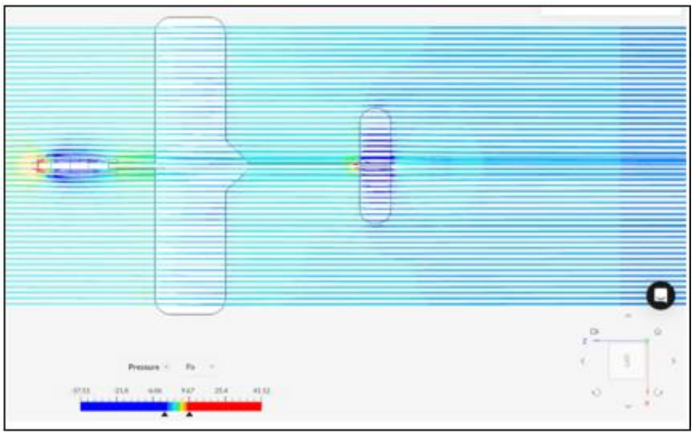

Figure 3: Pressure visualisation through contours at an AoA of 0°

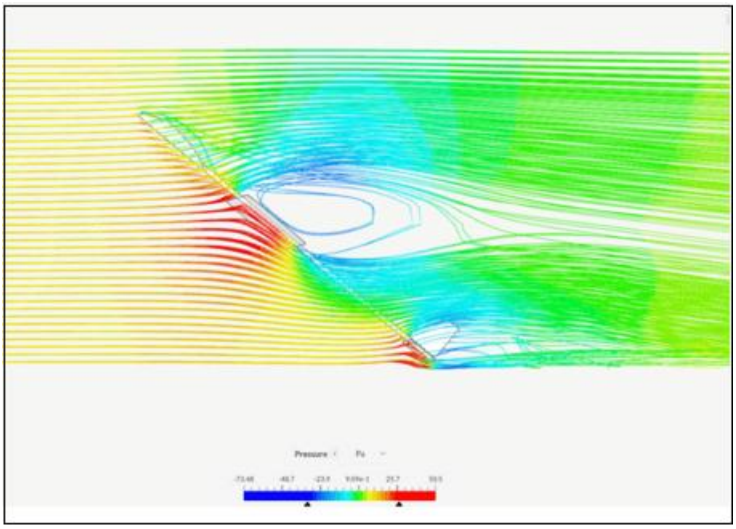

Figure 4: Flow separation and indication of Pressure Magnitude at an AoA of 30°

2. Methodology

This investigation employed a quantitative computational research methodology using CFD to evaluate the aerodynamic behaviour of a 3D-printed flat-plate glider across a range of angles of attack. Rather than relying on experimental wind-tunnel testing, numerical simulations were conducted to obtain the lift coefficient (CL), drag coefficient (CD), and aerodynamic efficiency (CL/CD). By varying only the angle of attack while maintaining all other parameters constant, the influence of angle of attack on aerodynamic performance and stall behaviour could be isolated.

CFD Setup

1) Domain

The domain for analysis and simulation had the following dimensions. They were chosen to be sufficiently large to minimise blockage.

- Height: 130mm
- Width: 450mm
- Breadth: 400mm

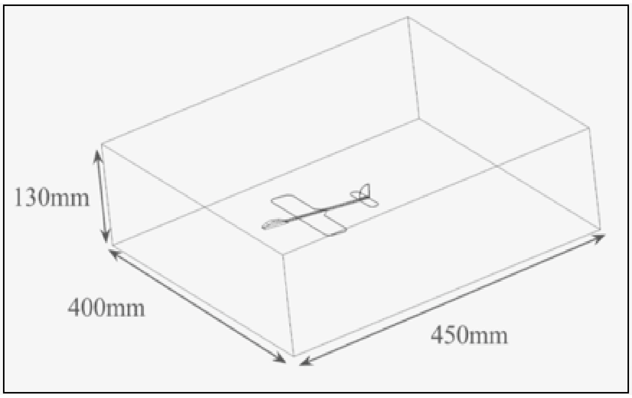

Figure 5: Dimensions of External Flow Volume Container given in millimeters (mm)

2) Boundary Conditions

- Fixed Value Velocity Inlet of 8m/s
- Fixed Value Zero Pressure Outlet at the rear end of the flow volume

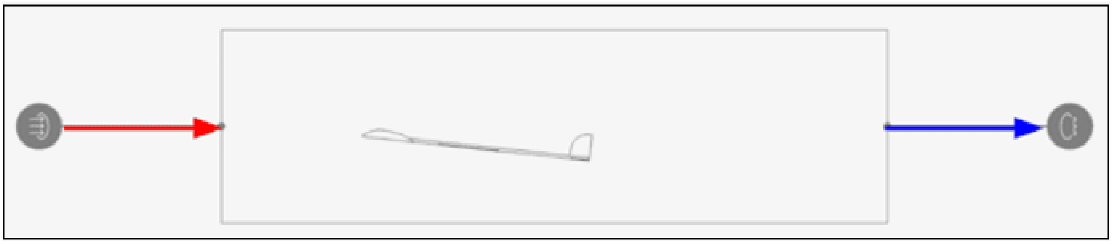

Figure 6: Side view visualisation of Velocity Entrance direction (denoted via red arrow) and Zero Pressure Outlet (denoted via blue arrow)

3) Solver

- The simulations were performed using the CFD solver available within SimScale. [20] A steady-state Reynolds Averaged Navier Stokes (RANS) approach was selected because the objective of the investigation was to determine the overall aerodynamic trends associated with changing angle of attack rather than capturing highly transient flow structures. [10,18]
- The k-ω Shear Stress Transport (SST) turbulence model was used for all simulations. This model was selected because it combines the advantages of the k-ω model near solid boundaries with the k-ε model in free-stream regions, providing improved prediction of adverse pressure gradients and flow separation. [11,18] Since the objective of this investigation was to identify the onset of stall, accurate representation of boundary-layer separation was essential.
- The simulation used air as the working fluid. Properties given in Table 3 (given ahead)

Paper ID: SR26729192930 DOI: https://dx.doi.org/10.21275/SR26729192930

- The inlet boundary condition was defined as a uniform velocity inlet with a magnitude of 8 m/s. The outlet boundary was defined as a pressure outlet with atmospheric pressure. The remaining external boundaries were assigned appropriate far-field or slip conditions to minimize interference between the computational domain and the airflow around the glider.
- The simulations were considered converged when the residuals reached a stable value of approximately 10^{-4} and the calculated aerodynamic coefficients showed negligible variation between subsequent iterations.

4) Mesh

- A computational mesh was generated around the glider using an automatic tetrahedral meshing approach within SimScale. [20] Local mesh refinement was applied around the wing surface, leading edge, and trailing edge regions due to the presence of strong pressure gradients and expected boundary-layer development.[13]
- The mesh density was increased near the glider surface to improve the accuracy of flow separation prediction, particularly near the stall region where small changes in airflow behaviour significantly affect lift and drag. [11,13]
- For each simulation, the aerodynamic coefficients were extracted after convergence was achieved. The primary outputs collected were the lift coefficient (CL) and drag coefficient (CD), as these parameters allow comparison of aerodynamic performance independent of the physical dimensions of the glider.

Table 2: Average Mesh Characteristics of all simulations

Parameter	Value (Average of all meshes)
Mesh type	Tetrahedral
Number of cells	≈1,200,000
Number of nodes	≈300,000
Number of Faces	≈2,600,000

Simulation Procedure

A series of steady-state CFD simulations were conducted to investigate the effect of angle of attack on the aerodynamic performance of the 3D-printed flat-plate glider. During each simulation, the glider geometry, fluid properties, mesh settings, turbulence model, and freestream velocity were maintained constant. The only parameter varied was the angle of attack, allowing its individual influence on aerodynamic behaviour to be isolated.

The angle of attack was varied from 0° to 30° in increments of 2°. This range was selected to capture the complete aerodynamic operating region of the glider, including the low-angle region where lift increases approximately linearly, the region of maximum aerodynamic efficiency, and the post-stall region where flow separation causes a reduction in lift. [1, 2, 9]

The freestream velocity was maintained at 8 m/s throughout all simulations to isolate the influence of angle of attack on aerodynamic performance while eliminating velocity as a confounding variable. This velocity is representative of the flight speed of lightweight hand-launched gliders operating at low Reynolds numbers and remains well below the compressibility limit of air, allowing incompressible flow assumptions to remain valid. Maintaining a constant velocity also ensured that changes in the lift coefficient, drag coefficient, and aerodynamic efficiency resulted solely from variations in angle of attack rather than changes in dynamic pressure.

An increment of 2° was selected as an appropriate compromise between simulation resolution and computational efficiency. Smaller angular increments would have increased the number of required simulations considerably while providing only marginal improvements in identifying the general aerodynamic trends. Conversely, larger increments could have reduced the accuracy with which the stall angle and the angle corresponding to maximum aerodynamic efficiency were identified. The chosen interval therefore provided sufficient resolution to capture the approximately linear pre-stall region, the onset of flow separation, and the post-stall behaviour while maintaining a practical computational cost.

Determination of Stall

The stall angle was determined using both quantitative aerodynamic data and confirmed with qualitative flow visualization.

The primary criterion used was the variation of lift coefficient with angle of attack. The stall angle was defined as the angle of attack corresponding to the maximum lift coefficient before a subsequent decrease in CL despite further increases in angle of attack. The relationship was identified from the CL versus angle of attack graph, where the peak value represented the transition from attached flow to stalled flow.

Near the stall angle, increased flow separation and disruption of the airflow over the wing surface were expected and were confirmed with streamlines for simulations AoA above the stall angle. At angles beyond stall, the separated region was expected to expand, resulting in reduced lift generation and increased aerodynamic drag.

Mesh independence: Three mesh densities were evaluated at an angle of attack of 10°. The medium and fine meshes produced CL and CD variations of less than 3%, therefore the medium mesh was selected as the optimal balance between computational cost and accuracy.[13]

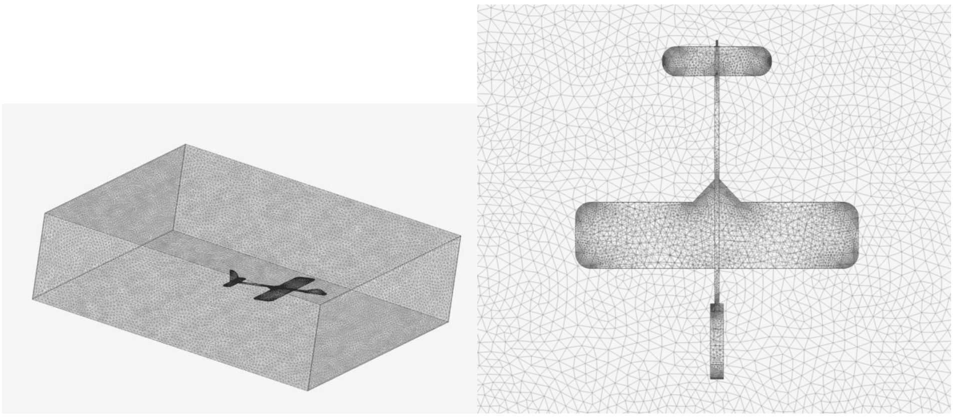

Figure 7: Example of Generated mesh for AoA of 10°.

Software Used
Onshape v1.218- CAD Modelling
SimScale 2026- CFD Simulation
Google Sheets- Graph Plotting
Google Docs- Report Writing

Boundary Conditions

Table 3: Fluid and Boundary Characteristics for all Simulations [12]

Parameter	Value
Air Density	1.196 kg/m³
Velocity	8 m/s
Pressure	Atmospheric
Temperature	273.15 K
Turbulence Model	k-ω SST
Fluid	Air

Table 4: Solver Settings

Setting	Value
Analysis Type	Steady State
Maximum Iterations	1000
Residual Target	10-Jul
Convergence	Yes

Source: SimScale Documentation [20]

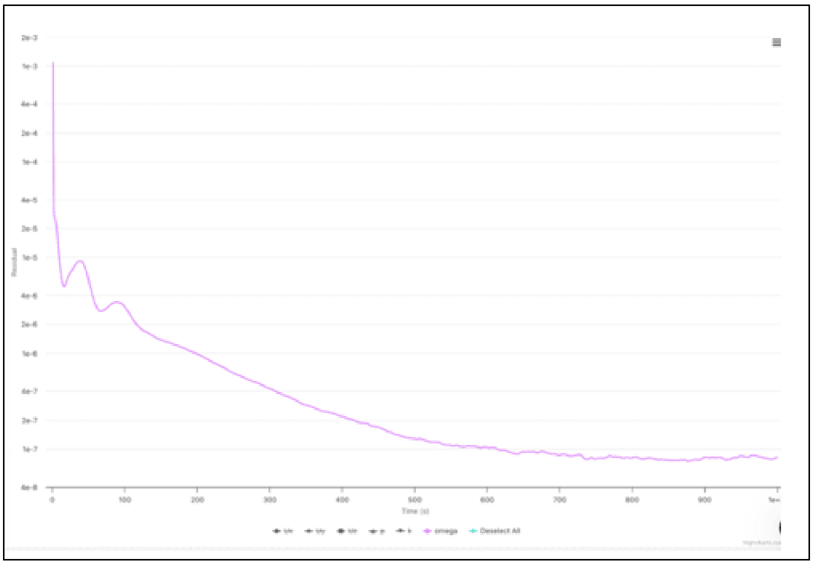

Figure 8: Residual Convergence graph of omega (ω) for simulation with AoA of 10°. The graph denotes a final residual of $\approx 10^{-7}$.

It is important to note that CL, CD and ω in all simulations converged similarly.

3. Results and Discussion

A total of 16 steady-state CFD simulations were conducted over an angle of attack range of 0° to 30° while maintaining constant freestream velocity, fluid properties, and glider geometry. For each simulation, the lift coefficient and drag coefficient were extracted directly from SimScale. Aerodynamic efficiency was subsequently calculated to identify the optimum operating angle for the glider. Pressure contours, velocity contours, and streamline visualizations were also obtained to examine changes in airflow behaviour as the angle of attack increased.

Table 5: Raw Simulation Data

AOA (°)	CL	CD	L/D
0	0.006	0.029	0.208
2	0.114	0.032	3.563
4	0.218	0.042	5.19
6	0.319	0.058	5.519
8	0.413	0.086	4.802
10	0.492	0.107	4.598
12	0.559	0.138	4.051
14	0.612	0.173	3.538
16	0.623	0.198	3.146
18	0.63	0.225	2.801
20	0.631	0.251	2.514
22	0.644	0.277	2.325
24	0.664	0.309	2.086
26	0.64	0.339	1.888
28	0.607	0.372	1.632
30	0.562	0.406	1.384

Data Analysis

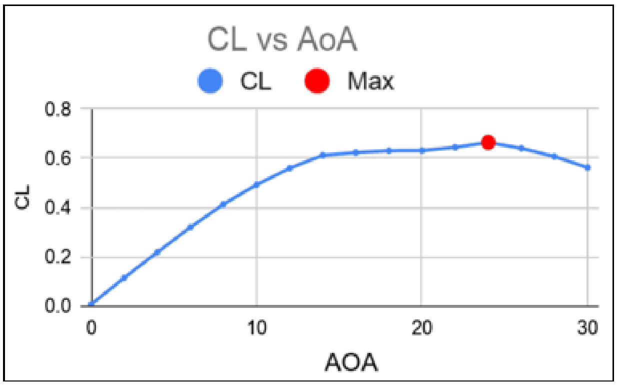

Figure 9: Line Graph showing the variation of CL with angle of attack.

Figure 9 illustrates the relationship between lift coefficient and angle of attack. Between 0° and 30°, CL increased approximately linearly from 0° to 12°, indicating efficient lift generation within the attached-flow regime. The maximum lift coefficient of 0.664 occurred at 26°, after which CL decreased despite further increases in angle of attack. This behaviour was taken as evidence of aerodynamic stall. [3, 9]

The lift curve slope within the pre-stall region was approximately constant, suggesting that the wing operated within its linear aerodynamic range. Beyond the stall angle, the reduction in lift indicated progressive flow separation over the upper surface.

Stall Angle

The stall angle was identified as 26°, corresponding to the maximum recorded lift coefficient. After this point, additional increases in angle of attack resulted in a reduction in lift despite increasing wing incidence. This behaviour is consistent with the aerodynamic definition of stall.

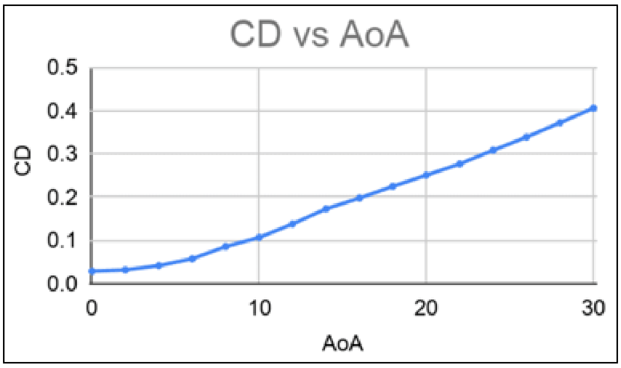

Figure 10: Straight line graph showing the variation of CD with angle of attack.

Figure 10 demonstrates that drag increased gradually at lower angles of attack before rising rapidly beyond 4°. The drag coefficient increased from 0.029 at 0° to 0.406 at 30°, representing an increase of approximately 1301.93%.

The nonlinear increase in drag suggests progressively stronger pressure drag associated with increasing flow separation. [3, 9, 17]

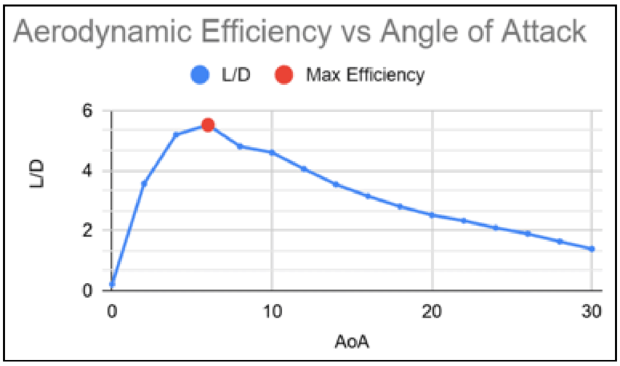

Figure 11: Straight Line graph showing the aerodynamic efficiency of the glider plotted against angle of attack.

Aerodynamic efficiency increased steadily between 0° and ≈6°, reaching a maximum CL/CD value of 5.519. Beyond this angle, aerodynamic efficiency decreased despite continued increases in lift coefficient, indicating that drag increased at a faster rate than lift.

The optimum glide condition therefore occurred at ≈6°, rather than at the stall angle. [3, 16, 21]

Pressure Contour Analysis

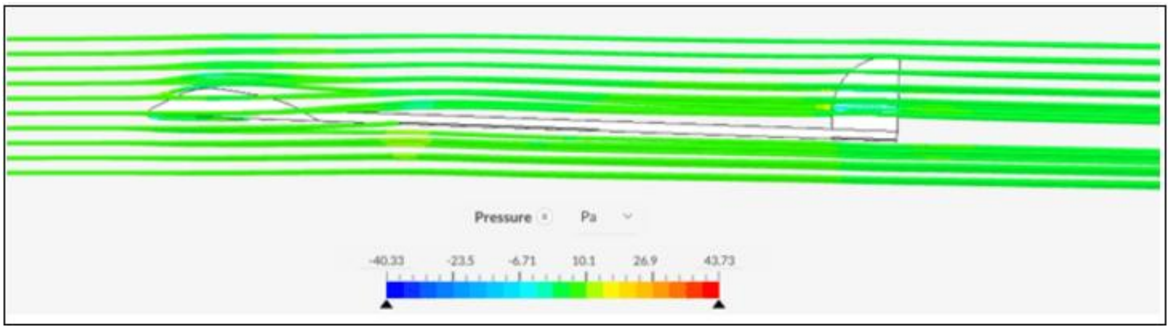

Figure 12: Pressure contour for AoA of 2°. At 2°, the pressure distribution was relatively symmetrical across the upper and lower wing surfaces, producing only a modest pressure differential and consequently limited lift generation. [3, 9]

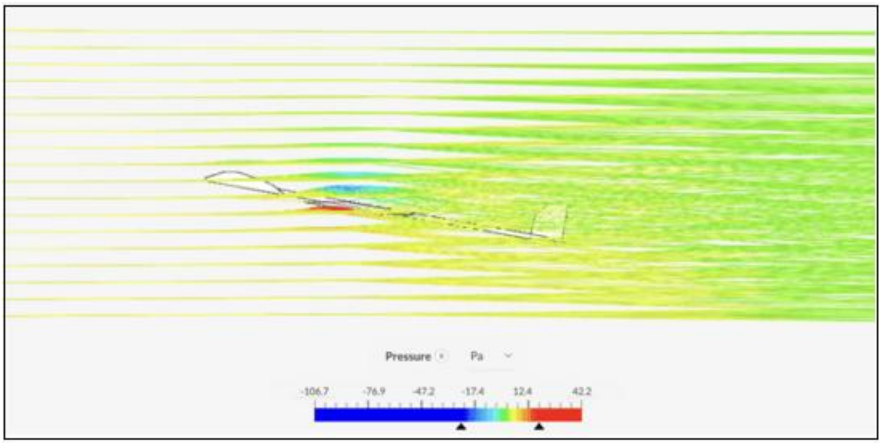

Figure 13: Pressure contour for AoA of 10°. At **10°**, the pressure difference between the upper and lower wing surfaces increased considerably, indicating stronger lift production. [3,9]

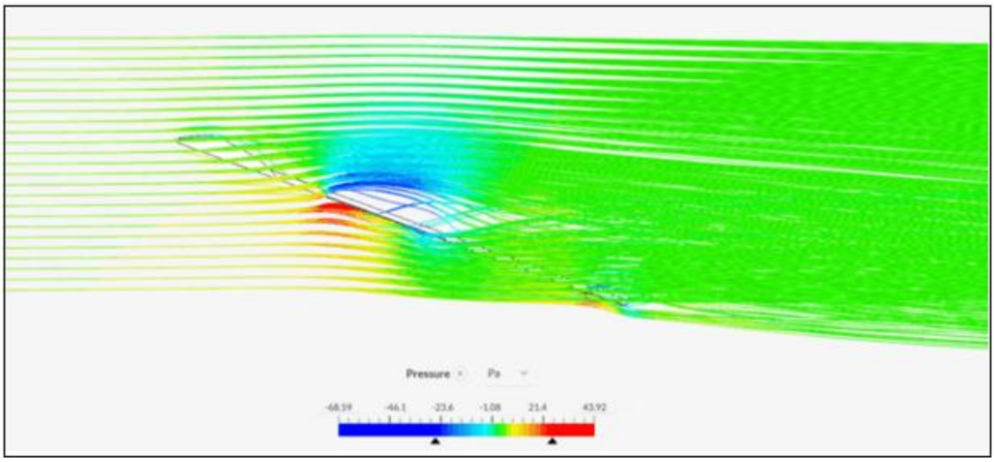

Figure 14: Pressure contour for AoA of 20°. Near the stall angle, a larger low-pressure region developed over the upper surface while localized pressure recovery near the trailing edge suggested the onset of flow separation. [3,9]

Paper ID: SR26729192930 DOI: https://dx.doi.org/10.21275/SR26729192930

ISSN: 2319-7064
Impact Factor 2025: 7.089

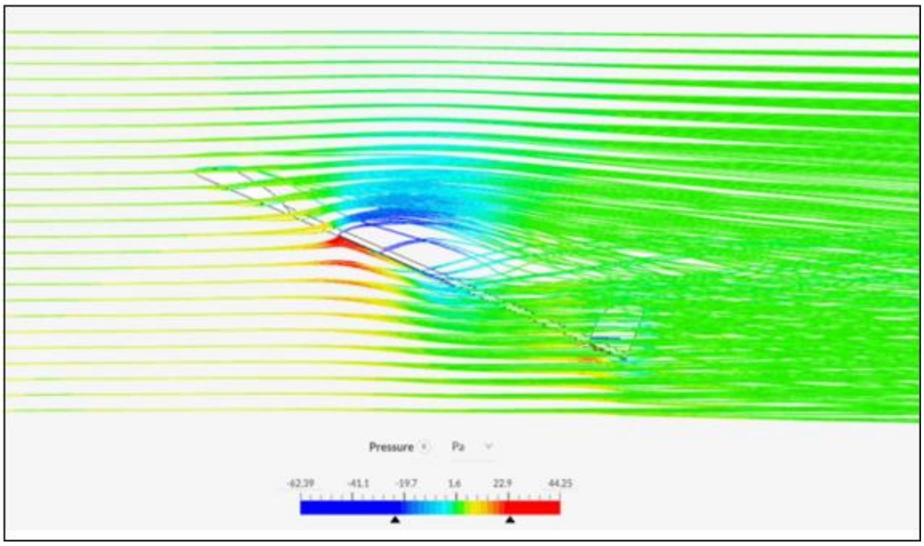

Figure 15 (a): Pressure contour for AoA of 22° side profile

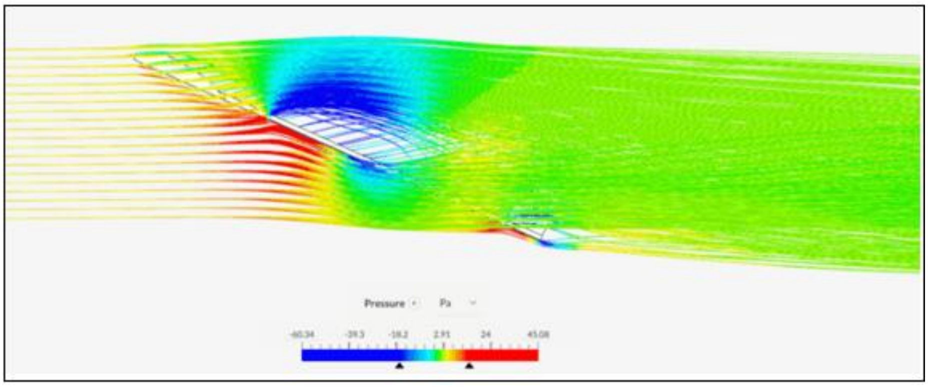

Figure 15(b): Pressure contour for AoA of 24° side profile.

Referencing figures 15a and 15b, near the stall angle, a larger low-pressure region developed over the upper surface while localized pressure recovery near the trailing edge suggested the onset of flow separation. [3,9]

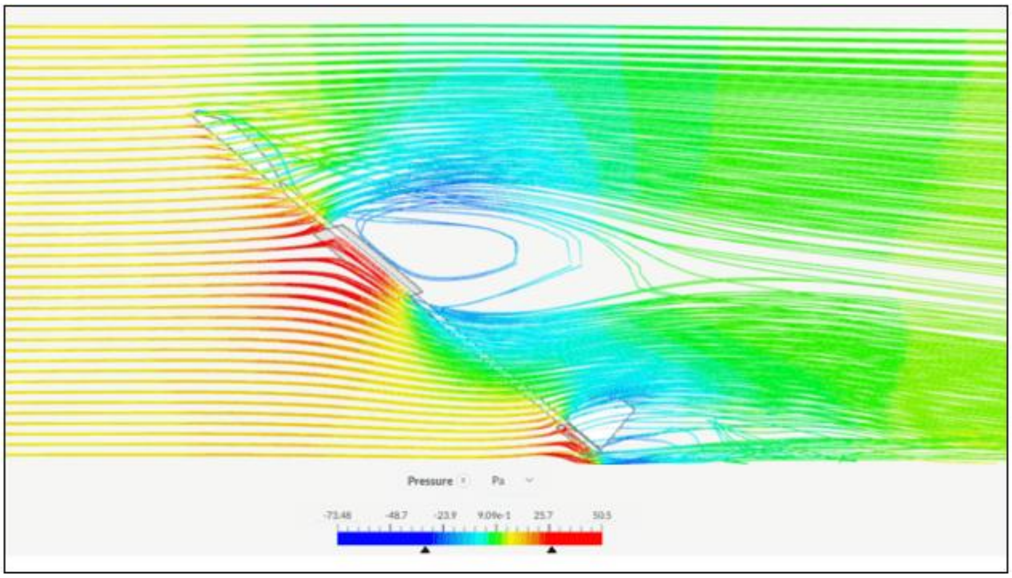

Figure 16: Pressure contour for AoA of 30°. Beyond stall, the pressure distribution became less uniform, consistent with reduced circulation around the wing. [3,9]

From figures 10, 11, 12, 13, 14, 15a, 15b and 16, we can verify that the larger pressure differential in each subsequent simulation explains the increasing lift coefficient observed between 2° and 26°.

Validation

The numerical results were compared with aerodynamic trends reported in previous studies on low-Reynolds-number flat-plate wings. These studies consistently report an approximately linear increase in lift coefficient in the pre-

Paper ID: SR26729192930 DOI: https://dx.doi.org/10.21275/SR26729192930

stall region, followed by a reduction in lift after the onset of flow separation, although the exact stall angle depends on Reynolds number, aspect ratio, wing geometry, and airfoil characteristics [1, 2, 3, 8, 9, 21, 22, 23].

Although the simulations successfully identified the overall aerodynamic trends associated with varying angle of attack, several limitations should be considered when interpreting the results. The investigation employed steady-state Reynolds-Averaged Navier–Stokes (RANS) simulations, which approximate the time-averaged flow field and therefore cannot fully capture the highly unsteady vortex shedding and transient flow structures that occur during stall. Furthermore, only a single glider geometry, freestream velocity, and Reynolds number were investigated, limiting the generalisability of the results to other wing configurations and operating conditions. The glider was also assumed to be perfectly rigid, neglecting structural deformation and manufacturing imperfections that may influence aerodynamic performance in practical flight. [5, 6, 10, 11, 18]

Several sources of numerical uncertainty are associated with the CFD methodology used in this investigation. Although a mesh independence study demonstrated that the medium and fine meshes produced lift and drag coefficient differences of less than 3%, discretisation errors remain unavoidable. Additional uncertainty arises from the assumptions inherent in the k–ω SST turbulence model, which approximates turbulent flow behaviour rather than resolving all turbulent structures directly. Minor numerical errors may also result from iterative convergence tolerances, boundary condition specification, and finite numerical precision. Consequently, while the absolute values of the calculated aerodynamic coefficients may contain small numerical uncertainties, the overall trends observed throughout the investigation are expected to remain reliable. [11,13]

Summary of Results

Table 9: Summary of the Results

Parameter	Result
Maximum CL	0.664
Maximum CD	0.406
Maximum CL/CD	5.53
Best Glide AoA	≈6°
Stall Angle	26°

The CFD simulations demonstrated a clear relationship between angle of attack and aerodynamic performance. Lift increased approximately linearly within the pre-stall region before reaching a maximum at 26°. [21,23] Drag increased continuously throughout the investigated range but accelerated rapidly beyond the onset of stall. [17] Aerodynamic efficiency reached its maximum at approximately 6°, indicating that the most efficient operating condition occurred prior to maximum lift generation.

4. Conclusion

Overall, the investigation demonstrates that CFD provides an effective method for analysing the aerodynamic behaviour of lightweight gliders during the conceptual design stage. [5, 6, 21] The methodology presented in this study may be applied to similar low-Reynolds-number aircraft and provides a foundation for future studies on wing optimisation and flight performance.

The investigation concludes that angle of attack has a significant influence on both aerodynamic efficiency and stall behaviour. Increasing angle of attack initially improves lift generation and aerodynamic efficiency by increasing the pressure differential across the wing. However, once a critical angle is exceeded, boundary-layer separation causes drag to increase rapidly while lift decreases, resulting in aerodynamic stall. [3, 9, 14] Consequently, optimum gliding performance is achieved at an angle of attack lower than the stall angle. [16]

Future investigations could extend this research by examining the influence of Reynolds number, wing aspect ratio, airfoil geometry, and freestream velocity on aerodynamic performance and stall behaviour. Experimental validation through wind-tunnel testing or controlled flight testing would provide an opportunity to quantify the accuracy of the numerical predictions and assess the suitability of the CFD methodology. Additionally, transient CFD simulations using Large Eddy Simulation (LES) or Detached Eddy Simulation (DES) could provide greater insight into the unsteady flow separation and vortex dynamics that occur during aerodynamic stall. Such investigations would contribute to the optimisation of lightweight gliders and other low-Reynolds-number aircraft used in educational, recreational, and micro air vehicle applications. [5,6,21]

References

[1] Gutierrez-Castillo P, Arredondo J, Campos-Amezcua R, et al. On the lift curve slope for rectangular flat plate wings at moderate Reynolds number. J Wind Eng Ind Aerodyn. 2021; 216: 104707.
[2] Ananda GK, Sukumar PP, Selig MS. Measured aerodynamic characteristics of wings at low Reynolds numbers. Aerosp Sci Technol. 2015; 42: 392-406.
[3] Anderson JD. Fundamentals of Aerodynamics. 7th ed. New York: McGraw-Hill Education; 2023.
[4] McLean D. Understanding Aerodynamics: Arguing from the Real Physics. Hoboken (NJ): Wiley; 2013.
[5] Ferziger JH, Perić M, Street RL. Computational Methods for Fluid Dynamics. 4th ed. Cham: Springer; 2020.
[6] Versteeg HK, Malalasekera W. An Introduction to Computational Fluid Dynamics: The Finite Volume Method. 2nd ed. Harlow: Pearson Education; 2007.
[7] Blazek J. Computational Fluid Dynamics: Principles and Applications. 3rd ed. Oxford: Elsevier; 2015.
[8] Mueller TJ, editor. Fixed and Flapping Wing Aerodynamics for Micro Air Vehicle Applications. Reston (VA): American Institute of Aeronautics and Astronautics; 2001.
[9] Abbott IH, von Doenhoff AE. Theory of Wing Sections. New York: Dover Publications; 1959.
[10] Wilcox DC. Turbulence Modeling for CFD. 3rd ed. La Cañada (CA): DCW Industries; 2006.

[11] Menter FR. Two-equation eddy-viscosity turbulence models for engineering applications. AIAA J. 1994;32(8):1598-1605.
[12] International Organization for Standardization. ISO 2533: Standard Atmosphere. Geneva: ISO; 1975.
[13] Roache PJ. Verification and Validation in Computational Science and Engineering. Albuquerque (NM): Hermosa Publishers; 1998.
[14] Schlichting H, Gersten K. Boundary-Layer Theory. 9th ed. Berlin: Springer; 2017.
[15] White FM. Fluid Mechanics. 9th ed. New York: McGraw-Hill Education; 2021.
[16] Anderson JD Jr. Introduction to Flight. 9th ed. New York: McGraw-Hill Education; 2021.
[17] Hoerner SF. Fluid-Dynamic Drag. Bakersfield (CA): Hoerner Fluid Dynamics; 1965.
[18] Pope SB. Turbulent Flows. Cambridge: Cambridge University Press; 2000.
[19] NASA Glenn Research Center. Beginner's Guide to Aerodynamics. Cleveland (OH): National Aeronautics and Space Administration; 2023.
[20] SimScale GmbH. SimScale Documentation: Incompressible CFD Analysis. Munich: SimScale GmbH; 2024.
[21] Drela M. Flight Vehicle Aerodynamics. Cambridge (MA): MIT Press; 2014.
[22] Lissaman PBS. Low-Reynolds-number airfoils. Annu Rev Fluid Mech. 1983; 15: 223-239.
[23] Liebeck RH. Design of subsonic airfoils for high lift. J Aircr. 1973;10(10):610-617.